General Theory for the Ferroelectric Polarization Induced by Spin-Spiral Order

H. J. Xiang,[1,*] E. J. Kan,[2] Y. Zhang,[3] M.-H. Whangbo,[3,†] and X. G. Gong[1,‡]

[1]*Key Laboratory of Computational Physical Sciences (Ministry of Education) and Department of Physics, Fudan University, Shanghai 200433, People's Republic of China*

[2]*Department of Applied Physics, Nanjing University of Science and Technology, Nanjing, Jiangsu 210094, People's Republic of China*

[3]*Department of Chemistry, North Carolina State University, Raleigh, North Carolina 27695-8204, USA*

(Received 19 July 2011; published 7 October 2011)

The ferroelectric polarization of triangular-lattice antiferromagnets induced by helical spin-spiral order is not explained by any existing model of magnetic-order-driven ferroelectricity. We resolve this problem by developing a general theory for the ferroelectric polarization induced by spin-spiral order and then by evaluating the coefficients needed to specify the general theory on the basis of density functional calculations. Our theory correctly describes the ferroelectricity of triangular-lattice antiferromagnets driven by helical spin-spiral order and incorporates known models of magnetic-order-driven ferroelectricity as special cases.

DOI: 10.1103/PhysRevLett.107.157202 PACS numbers: 75.85.+t, 71.20.−b

Multiferroics, displaying magnetic, polar, and elastic order parameters simultaneously, present fascinating fundamental physics [1,2] and potentially promising applications [3]. Spin-spiral multiferroics [1,4,5] constitute a challenging and interesting class of ferroelectricity in which the ferroelectric polarization $\mathbf{P}$ is induced by a magnetic order that removes inversion symmetry. For multiferroics with cycloidal spin-spiral order (e.g., $TbMnO_3$ [6–8] and $MnWO_4$ [9,10]), the ferroelectricity is explained by the inverse Dzyaloshinskii-Moriya interaction [11] or, equivalently, by the spin current model of Katsura, Nagaosa, and Balatsky (KNB) [12], leading to $\mathbf{P}_{ij} \propto \mathbf{e}_{ij} \times (\mathbf{S}_i \times \mathbf{S}_j)$, where $\mathbf{e}_{ij}$ is a unit vector connecting the two adjacent spins $\mathbf{S}_i$ and $\mathbf{S}_j$. This model predicts that $\mathbf{P}$ is perpendicular to the direction of the magnetic modulation $\mathbf{q} \propto \mathbf{e}_{ij}$ (i.e., $\mathbf{P} \perp \mathbf{q}$). Triangular-lattice antiferromagnets such as $CuFeO_2$ and $AgCrO_2$ also exhibit ferroelectricity when they adopt a helical spin-spiral order [13–15], in which the plane of the spin rotation is perpendicular to $\mathbf{q}$. $CuFeO_2$ shows ferroelectric polarization when its magnetic structure has a helical spin-spiral order with $\mathbf{q} = (Q, Q, 0)$, where $Q \approx 1/3$. The layered iodide MnI_2 was also found to be a multiferroic with helical spin-spiral order [16]. The experimental studies on $CuFeO_2$ and MnI_2 show that the $\mathbf{P}$ in the helical spin-spiral state with $\mathbf{q} = (Q, Q, 0)$ is parallel to $\mathbf{q}$ (i.e., $\mathbf{P} || \mathbf{q}$). This finding is not explained either by the symmetric exchange striction mechanism or by the KNB model. The charge transfer between metal and a ligand induced by spin-orbit coupling (SOC) was considered responsible for the ferroelectric polarization in a triangular lattice with helical spin-spiral order [17] with the prediction $\mathbf{P}_{ij} \propto (\mathbf{e}_{ij} \cdot \mathbf{S}_i)\mathbf{S}_i - (\mathbf{e}_{ij} \cdot \mathbf{S}_j)\mathbf{S}_j$. This polarization, known as the "bond polarization" [18], lies in the plane spanned by $\mathbf{S}_i$ and $\mathbf{S}_j$, which is perpendicular to $\mathbf{q}$, and hence contradicts the experimental observation [14,16,19] that $\mathbf{P} || \mathbf{q}$ when $\mathbf{q} = (Q, Q, 0)$. In short, to explain the ferroelectric polarization of triangular-lattice antiferromagnets with helical spin-spiral order, it is necessary to develop a general theory for the ferroelectric polarization driven by spin-spiral order.

In this Letter, we resolve the aforementioned issue first by developing a general theory for the ferroelectric polarization induced by spin spiral on the basis of symmetry considerations and then by evaluating the coefficients needed to specify the general theory on the basis of density functional calculations for MnI_2 as a representative example. We demonstrate that our theory correctly describes the ferroelectric polarization of MnI_2, and the existing models of magnetic-order-driven ferroelectricity are special cases of our theory.

Let us first consider a spin dimer (i.e., a pair of adjacent spin sites) with spatial inversion symmetry at the center. Without loss of generality, the distance vector from spin 1 to spin 2 will be taken along the x axis. A noncollinear spin arrangement of the dimer removes the inversion symmetry and hence induces ferroelectric polarization $\mathbf{P}$. In general, $\mathbf{P}$ is a function of the directions of spin 1 and spin 2 (with unit vectors $\mathbf{S}_1$ and $\mathbf{S}_2$, respectively), namely, $\mathbf{P} = \mathbf{P}(S_{1x}, S_{1y}, S_{1z}, S_{2x}, S_{2y}, S_{2z})$. In principle, therefore, $\mathbf{P}$ can be expanded as a Taylor series of $S_{i\alpha}$ ($i = 1, 2$; $\alpha = x, y, z$). The time-reversal symmetry requires that inverting both spin directions leave the electric polarization unchanged. Thus, the odd terms of the Taylor expansion should vanish. If the fourth and higher order terms are neglected, $\mathbf{P}$ is written as

$$\mathbf{P} = \mathbf{P}_1(\mathbf{S}_1) + \mathbf{P}_2(\mathbf{S}_2) + \mathbf{P}_{12}(\mathbf{S}_1, \mathbf{S}_2), \quad (1)$$

where the intrasite polarization $\mathbf{P}_i(\mathbf{S}_i)$ ($i = 1, 2$) and the intersite polarization $\mathbf{P}_{12}(\mathbf{S}_1, \mathbf{S}_2)$ are given by

$$\mathbf{P}_i(\mathbf{S}_i) = \sum_{\alpha\beta} \mathbf{P}_i^{\alpha\beta} S_{i\alpha} S_{i\beta},$$
$$\mathbf{P}_{12}(\mathbf{S}_1, \mathbf{S}_2) = \sum_{\alpha\beta} \mathbf{P}_{12}^{\alpha\beta} S_{1\alpha} S_{2\beta}. \quad (2)$$

Here the expansion coefficients $\mathbf{P}_i^{\alpha\beta}$ and $\mathbf{P}_{12}^{\alpha\beta}$ are vectors. The above expressions show that $\mathbf{P}_i^{\alpha\beta} = \mathbf{P}_i^{\beta\alpha}$, $\mathbf{P}_i(\mathbf{S}_i) = \mathbf{P}_i(-\mathbf{S}_i)$, and $\mathbf{P}_{12}(-\mathbf{S}_1, \mathbf{S}_2) = \mathbf{P}_{12}(\mathbf{S}_1, -\mathbf{S}_2) = -\mathbf{P}_{12}(\mathbf{S}_1, \mathbf{S}_2)$. From these relationships, together with the use of spatial inversion symmetry and time-reversal symmetry, one can show that $\mathbf{P}_1^{\alpha\beta} = -\mathbf{P}_2^{\alpha\beta}$ and $\mathbf{P}_{12}^{\alpha\beta} = -\mathbf{P}_{12}^{\beta\alpha}$ [20]. The latter relation shows that the diagonal coefficients $\mathbf{P}_{12}^{\alpha\alpha} = 0$, so the intersite polarization can be expressed as

$$\mathbf{P}_{12} = \mathbf{P}_{12}^{yz}(\mathbf{S}_1 \times \mathbf{S}_2)_x + \mathbf{P}_{12}^{zx}(\mathbf{S}_1 \times \mathbf{S}_2)_y + \mathbf{P}_{12}^{xy}(\mathbf{S}_1 \times \mathbf{S}_2)_z, \quad (3a)$$

where $(\mathbf{S}_1 \times \mathbf{S}_2)_\alpha$ refers to the $\alpha(= x, y, z)$ component of the vector $(\mathbf{S}_1 \times \mathbf{S}_2)$. By using similar notations for the x, y, and z components of the vectors $\mathbf{P}_{12}^{\alpha\beta}$, Eq. (3a) is rewritten as

$$\mathbf{P}_{12} = \mathbf{M}(\mathbf{S}_1 \times \mathbf{S}_2) \quad (3b)$$

with the 3×3 matrix $\mathbf{M}$:

$$\mathbf{M} = \begin{bmatrix} (\mathbf{P}_{12}^{yz})_x & (\mathbf{P}_{12}^{zx})_x & (\mathbf{P}_{12}^{xy})_x \\ (\mathbf{P}_{12}^{yz})_y & (\mathbf{P}_{12}^{zx})_y & (\mathbf{P}_{12}^{xy})_y \\ (\mathbf{P}_{12}^{yz})_z & (\mathbf{P}_{12}^{zx})_z & (\mathbf{P}_{12}^{xy})_z \end{bmatrix}. \quad (4)$$

Given that the distance vector from spin 1 to spin 2 is taken along the x axis, the bond polarization model [18] is a special case of the intrasite polarization in which the only nonzero coefficients are $\mathbf{P}_1^{xx} = (C, 0, 0)$, $\mathbf{P}_1^{xy} = \mathbf{P}_1^{yx} = (0, C/2, 0)$, and $\mathbf{P}_1^{zx} = \mathbf{P}_1^{xz} = (0, 0, C/2)$, where C is a constant. The KNB model is a special case of the intersite polarization with $(\mathbf{P}_{12}^{zx})_z = -(\mathbf{P}_{12}^{xy})_y = C$ as the only nonzero elements of $\mathbf{M}$, where C is a constant. The intersite polarization given by Eq. (3b) may now be referred to as the generalized KNB (gKNB) model. For a linear three-atom $M-L-M$ model (M = transition metal, L = main-group ligand), the intrasite term reduces to the bond polarization model and the intersite term to the KNB model.

To specify the intrasite and intersite polarizations described above, one needs to determine the expansion coefficients $\mathbf{P}_i^{\alpha\beta}$ ($i = 1, 2$) and $\mathbf{P}_{12}^{\alpha\beta}$. We evaluate these coefficients for a spin dimer of MnI_2 [Fig. 1(a)] as a representative example, on the basis of density functional calculations. We adopt the LDA + U + SOC approach to calculate electric polarizations [20]. MnI_2 crystallizes in the CdI_2-type structure with MnI_2 layers stacked along the c axis [see the left inset in Fig. 1(a)]. In the Mn triangular lattice, each Mn^{2+} ion has six nearest neighbor (NN) Mn^{2+} ions. The structure of an isolated Mn_2I_{10} cluster (i.e., a spin dimer), namely, an isolated Mn-Mn pair plus its 10 first-coordinate I atoms, is shown in the upper-right inset in Fig. 1(a). Each NN Mn-Mn pair contributes to the total electric polarization. To characterize the ferroelectric polarization arising from one pair of NN Mn^{2+} ions in MnI_2, we isolate a Mn-Mn pair in a $5 \times 5 \times 1$ supercell of MnI_2 and replace all other Mn^{2+} ions with nonmagnetic Mg^{2+} ions, as depicted in Fig. 1(a). (A more accurate method for calculating the coefficients of the intersite term requires no substitution of Mn^{2+} ions with nonmagnetic ions such as Mg^{2+} ions [20] and will be referred to as the no-substitution method.) When the SOC effect is excluded in the density functional calculations, the electric polarizations become zero so that the SOC effect is essential for the occurrence of ferroelectricity in helical spin-spiral systems.

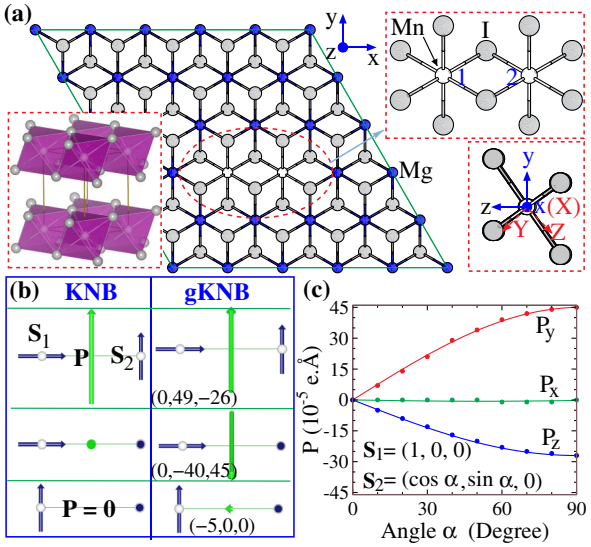

FIG. 1 (color online). (a) The $5 \times 5 \times 1$ supercell of MnI_2 in which all Mn^{2+} ions except for an isolated NN Mn-Mn pair are replaced by nonmagnetic Mg^{2+} ions. The left inset illustrates the layered structure of MnI_2. The upper-right inset shows the top view of the Mn_2I_{10} dimer cluster. The lower-right inset shows the local coordinate systems (x, y, z) and (X, Y, Z) employed for calculations. (b) The electric polarizations predicted by the KNB and gKNB models for three different spin configurations of the Mn-Mn dimer, where the directions of the spins and the polarizations are described in terms of the (x, y, z) coordinate system shown in Fig. 1(a). The blue dots representing $\mathbf{S}_2$ mean that it is pointed along the positive z axis, and so does the green dot representing the polarization in the KNB model. The Cartesian components of the polarizations obtained from the gKNB model are given in units of 10^{-5} eÅ. (c) The polarization of the Mn-Mn pair with spins in the xy plane as a function of the angle α between the spins $\mathbf{S}_1$ and $\mathbf{S}_2$. The data points were obtained from direct density functional calculations and the solid curves from the model of Eq. (1).

The expansion coefficients $\mathbf{P}_i^{\alpha\beta}$ ($i = 1, 2$) and $\mathbf{P}_{12}^{\alpha\beta}$ for a given spin dimer can be readily determined by mapping analysis once its polarizations are calculated for a set of carefully chosen noncollinear spin arrangements. To

TABLE I. The four spin arrangements I′–IV′ of the spin dimer employed to calculate its off-diagonal intrasite electric polarization $\mathbf{P}_1^{xy}$ by LDA + U + SOC calculations.

	$\mathbf{S}_1$	$\mathbf{S}_2$
I′	$(\sqrt{2}/2, \sqrt{2}/2, 0)$	$(1, 0, 0)$
II′	$(\sqrt{2}/2, \sqrt{2}/2, 0)$	$(-1, 0, 0)$
III′	$(\sqrt{2}/2, \sqrt{2}/2, 0)$	$(1, 0, 0)$
IV′	$(\sqrt{2}/2, \sqrt{2}/2, 0)$	$(-1, 0, 0)$

evaluate an off-diagonal coefficient of the intrasite polarization, for example, $\mathbf{P}_1^{xy}$, we calculate the electric polarizations for the four spin arrangements I′–IV′ of the spin dimer specified in Table I. Then, according to Eq. (2), $\mathbf{P}_1^{xy}$ is related to the polarization of the spin arrangements I′–IV′ as $\mathbf{P}_1^{xy} = (\mathbf{P}_{\mathrm{I}'} + \mathbf{P}_{\mathrm{II}'} - \mathbf{P}_{\mathrm{III}'} - \mathbf{P}_{\mathrm{IV}'})/4$. Other off-diagonal intrasite coefficients, $\mathbf{P}_1^{xz}$ and $\mathbf{P}_1^{yz}$, can be evaluated in a similar manner [20]. The diagonal coefficients of the intrasite polarization can be determined by calculating the electric polarizations for the six spin arrangements I–VI of the spin dimer specified in Table II. According to Eq. (2), the polarizations of these spin arrangements have the relationships $\mathbf{P}_{\mathrm{I}} + \mathbf{P}_{\mathrm{II}} = 2(\mathbf{P}_1^{xx} - \mathbf{P}_1^{yy})$, $\mathbf{P}_{\mathrm{III}} + \mathbf{P}_{\mathrm{IV}} = 2(\mathbf{P}_1^{xx} - \mathbf{P}_1^{zz})$, and $\mathbf{P}_{\mathrm{V}} + \mathbf{P}_{\mathrm{VI}} = 2(\mathbf{P}_1^{yy} - \mathbf{P}_1^{zz})$. Two of these three equations are linearly independent, but only the two independent parameters $(\mathbf{P}_1^{xx} - \mathbf{P}_1^{yy})$ and $(\mathbf{P}_1^{xx} - \mathbf{P}_1^{zz})$ are needed in calculating the sum of the diagonal contributions of the two intrasite polarizations because of the relationship $\mathbf{P}_1^{\alpha\beta} = -\mathbf{P}_2^{\alpha\beta}$ [20]. The electric polarizations of the above six spin arrangements can also be used to extract the coefficients of the intersite polarization $\mathbf{P}_{12}$, that is, $\mathbf{P}_{12}^{xy} = (\mathbf{P}_{\mathrm{I}} - \mathbf{P}_{\mathrm{II}})/2$, $\mathbf{P}_{12}^{xz} = (\mathbf{P}_{\mathrm{III}} - \mathbf{P}_{\mathrm{IV}})/2$, and $\mathbf{P}_{12}^{yz} = (\mathbf{P}_{\mathrm{V}} - \mathbf{P}_{\mathrm{VI}})/2$ [20].

Our calculations for the spin dimer of MnI_2 and mapping analyses as outlined above show that the coefficients of the intrasite polarization are $\mathbf{P}_1^{xx} = (0, 0, 0)$, $\mathbf{P}_1^{yy} = (2.5, 0, 0)$, $\mathbf{P}_1^{zz} = (-2.5, 0, 0)$, $\mathbf{P}_1^{xy} = (5.0, 7.5, 0)$, $\mathbf{P}_1^{xz} = (0, -5.0, 0)$, and $\mathbf{P}_1^{yz} = (7.5, -2.5, 0)$ in units of 10^{-6} eÅ. Note that the expression of the intrasite polarization differs from that of the bond polarization model (see above). The coefficients

TABLE II. The six spin arrangements I–VI of the spin dimer employed to calculate its diagonal intrasite electric polarization $\mathbf{P}_1^{\alpha\alpha}$ $(\alpha = x, y, z)$ as well as the intersite polarization $\mathbf{P}_{12}^{xy}$, $\mathbf{P}_{12}^{xz}$, and $\mathbf{P}_{12}^{yz}$ by LDA + U + SOC calculations.

	$\mathbf{S}_1$	$\mathbf{S}_2$
I	$(1, 0, 0)$	$(0, 1, 0)$
II	$(1, 0, 0)$	$(0, -1, 0)$
III	$(1, 0, 0)$	$(0, 0, 1)$
IV	$(1, 0, 0)$	$(0, 0, -1)$
V	$(0, 1, 0)$	$(0, 0, 1)$
VI	$(0, 1, 0)$	$(0, 0, -1)$

of the intersite polarization extracted by using the no-substitution method [20] are

$$M = \begin{bmatrix} M_{11} & 0 & 0 \\ 0 & M_{22} & M_{23} \\ 0 & M_{32} & M_{33} \end{bmatrix}, \tag{5}$$

where, in units of 10^{-5} eÅ, $\mathrm{M}_{11} = -4.8$, $\mathrm{M}_{22} = 39.5$, $\mathrm{M}_{23} = 49.0$, $\mathrm{M}_{32} = -44.5$, and $\mathrm{M}_{33} = -26.0$. Thus, the intersite polarization is at least an order of magnitude stronger than the intrasite polarization and differs from the KNB model (see above) because the matrix elements $\mathrm{M}_{11} = (\mathbf{P}_{12}^{yz})_x$, $\mathrm{M}_{22} = (\mathbf{P}_{12}^{zx})_y$, and $\mathrm{M}_{33} = (\mathbf{P}_{12}^{xy})_z$ are not zero and because $\mathrm{M}_{23} = (\mathbf{P}_{12}^{xy})_y$ is different from $-\mathrm{M}_{32} = -(\mathbf{P}_{12}^{zx})_z$. Figure 1(b) illustrates the differences between the KNB and gKNB models in predicting the polarization $\mathbf{P}$ for three different spin arrangements of the Mn-Mn dimer. Given the expansion coefficients $\mathbf{P}_{12}^{\alpha\beta}$ extracted as described above, one can predict the $\mathbf{P}$ of the Mn-Mn dimer with various spin arrangements by using Eq. (1). To show that the gKNB model can indeed predict the $\mathbf{P}$ of the Mn-Mn pair with arbitrary spin orientations, we compute $\mathbf{P}$ for several spin arrangements of the Mn-Mn dimer directly from density functional calculations. For convenience, we keep the first Mn spin along the x direction and rotate the second Mn spin in the xy plane in these spin arrangements. Then, the $\mathbf{P}$ is found to lie in the yz plane. Importantly, the polarization predicted by the gKNB model is in excellent agreement with the value calculated directly from density functional calculations for the spin dimer [see Fig. 1(c)]. This validates our analysis of the electric polarization without considering the fourth and higher order terms.

With the electric polarizations calculated for various NN Mn-Mn pairs, we now estimate the electric polarization of MnI_2 with helical spin-spiral order in terms of only the intersite term, because the sum of all intrasite terms for any helical spin-spiral arrangement is zero. Since each Mn spin site i has six NN Mn spins $k(= 1\text{–}6)$, the total polarization $\mathbf{P}_i^{\mathrm{tot}}$ at the site i is written as $\mathbf{P}_i^{\mathrm{tot}} = \sum_{k=1}^{6} \mathbf{P}_{ik}$. In the case of spin spiral, $\mathbf{P}_i^{\mathrm{tot}}$ is the same for all i sites, so we consider only the polarization associated with site 0 shown in Fig. 2(a), for which $\mathbf{P}_i^{\mathrm{tot}} = \sum_{k=1}^{6} \mathbf{P}_{0k} = \sum_{k=1}^{6} \mathbf{M}^{0k}(\mathbf{S}_0 \times \mathbf{S}_k)$, where $\mathbf{M}^{0k}$ refers to the matrix for the intersite polarization for pair 0 and k. In the local (x, y, z) coordinate system defined in Fig. 1(a), our calculations show that for $\mathbf{q} = (Q, 0, 0)$, $\mathbf{P}_0^{\mathrm{tot}} = (\sqrt{3}/2\mathrm{A}, -\frac{3}{2}\mathrm{A}, 0)$ with $\mathrm{A} = (\mathrm{M}_{11} - \mathrm{M}_{22}) \sin 2\pi Q$. In the case of $\mathbf{q} = (Q, Q, 0)$, $\mathbf{P}_0^{\mathrm{tot}} = (\frac{1}{2}\mathrm{B}, \sqrt{3}/2\mathrm{B}, 0)$ with $\mathrm{B} = (\mathrm{M}_{11} + 3\mathrm{M}_{22} - 4\mathrm{M}_{11} \cos 2\pi Q) \sin 2\pi Q$. Thus, the gKNB model predicts that $\mathbf{P} \perp \mathbf{q}$ when $\mathbf{q} = (Q, 0, 0)$, but $\mathbf{P} \| \mathbf{q}$ in the case of $\mathbf{q} = (Q, Q, 0)$, as found experimentally [16], and that the polarization reverses with the change in the spin chirality ($\mathbf{q}$ to $-\mathbf{q}$), in accord with experiment. The gKNB model shows that the polarization in both cases depends only on two elements of

the matrix **M**, i.e., M_{11} and M_{22}, both of which are zero in the KNB model. In Fig. 2(b), we plot the magnitude of the polarization as a function of Q for the cases of $\mathbf{q} = (Q, 0, 0)$ and $\mathbf{q} = (Q, Q, 0)$. The plot is symmetric with maximum at $Q = 0.25$ in the case of $\mathbf{q} = (Q, 0, 0)$ but is slightly asymmetric with maximum at $Q = 0.225$ in the case of $\mathbf{q} = (Q, Q, 0)$.

We determine the total ferroelectric polarization of MnI_2 in the helical spin-spiral state with $\mathbf{q} = (0.181, 0, 0.439)$, observed in the absence of an applied magnetic field, directly from density functional calculations by approximating the incommensurate state with the commensurate helical spin-spiral state with $\mathbf{q} = (1/3, 0, 0)$ by using a $3 \times 1 \times 1$ supercell. Our calculations show that the electric polarization of this state is 58.8 $\mu C/m^2$ along the [100] direction, as shown in Fig. 2(a). Thus, our density functional calculations show that $\mathbf{P} \perp \mathbf{q}$, in agreement with experiment [16]. For the helical spin-spiral state of MnI_2 with $\mathbf{q} = (Q, Q, 0)$, found under an in-plane magnetic field greater than 3 T [16], we use a $\sqrt{3} \times \sqrt{3} \times 1$ supercell to simulate the $\mathbf{q} = (1/3, 1/3, 0)$ state. The total polarization of this state is calculated to be 71.4 $\mu C/m^2$ along the [110] direction. In this case, $\mathbf{P} \| \mathbf{q}$, again in agreement with experiment [16]. As can be seen from Figs. 2(c) and 2(d), the gKNB model not only predicts the correct direction of the polarization but also gives a rather accurate magnitude of the polarization for the cases of $\mathbf{q} = (Q, 0, 0)$ and $\mathbf{q} = (Q, Q, 0)$. Our theory of ferroelectric polarization is general and is expected to provide accurate predictions when applied to other multiferroics driven by spin-spiral magnetic order.

In the local coordinate system (X, Y, Z) chosen to minimize the magnitudes of the diagonal elements of the matrix **M** [see the lower-right inset in Fig. 1(a); the Y axis is close to the distance vector between the two I atoms forming the shared octahedral edge between the adjacent Mn atoms], the matrix **M** of Eq. (5) determined from density functional calculations is rewritten as

$$\mathbf{M} = \begin{bmatrix} -4.8 & 0 & 0 \\ 0 & 6.8 & 79.6 \\ 0 & -13.9 & 6.8 \end{bmatrix} \quad (6)$$

in units of 10^{-5} eÅ. In the local (X, Y, Z) coordinate system, $(\mathbf{P}_{12}^{XY})_Y = 79.6 \times 10^{-5}$ eÅ is much greater than $-(\mathbf{P}_{12}^{ZX})_Z = 13.9 \times 10^{-5}$ eÅ. The cause for this anisotropy was examined by performing tight-binding calculations for a planar M_2L_2 cluster consisting of two transition metal atoms M bridged by two ligand atoms L [20] on the basis of the model Hamiltonian similar to that employed by Jia *et al.* [18]. This analysis shows [20] that the large difference between $(\mathbf{P}_{12}^{XY})_Y$ and $-(\mathbf{P}_{12}^{ZX})_Z$ arises from the structural anisotropy of the planar M_2L_2 cluster; the Y axis is nearly in the plane of, but the Z axis is nearly perpendicular to, the plane of the cluster.

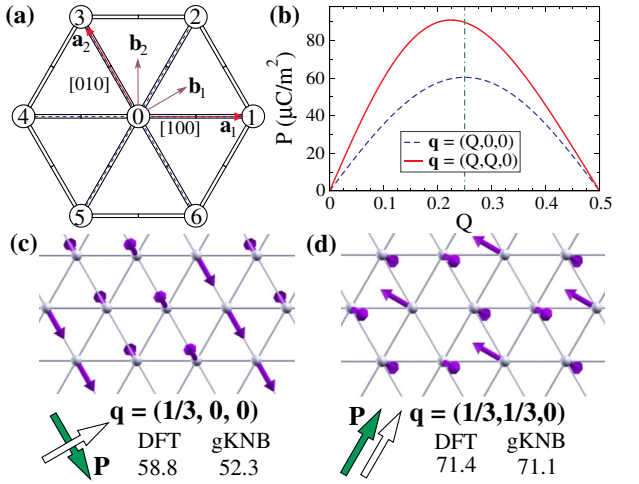

FIG. 2 (color online). (a) The triangular lattice of Mn^{2+} ions, where the in-plane lattice vectors a_1 and a_2 and the corresponding reciprocal lattice vectors b_1 and b_2 are shown. (b) The magnitude of the polarization predicted from our gKNB model as a function of Q for the cases of $\mathbf{q} = (Q, 0, 0)$ and $\mathbf{q} = (Q, Q, 0)$. (c),(d) The spin orientations of two proper-screw spirals with $\mathbf{q} = (1/3, 0, 0)$ and $\mathbf{q} = (1/3, 1/3, 0)$. The modulation vector **q** and the polarization vector **P** are represented by the white and green arrows, respectively. The numbers (in $\mu C/m^2$) denote the magnitudes of the polarizations obtained from the direct density functional calculation and the gKNB model.

In summary, on the basis of symmetry arguments, we developed a general theory of ferroelectric polarization that can correctly describe all known ferroelectric polarization induced by spin-spiral order.

Work at Fudan was partially supported by NSFC, Pujiang plan, and Program for Professor of Special Appointment (Eastern Scholar).

*hxiang@fudan.edu.cn
†mike_whangbo@ncsu.edu
‡xggong@fudan.edu.cn

[1] S.-W. Cheong and M. Mostovoy, Nature Mater. **6**, 13 (2007); R. Ramesh and N. Spaldin, Nature Mater. **6**, 21 (2007); S. Picozzi and C. Ederer, J. Phys. Condens. Matter **21**, 303201 (2009).
[2] K. Wang, J.-M. Liu, and Z. Ren, Adv. Phys. **58**, 321 (2009).
[3] M. Bibes, J. E. Villegas, and A. Barthélémy, Adv. Phys. **60**, 5 (2011).
[4] T. Kimura, Annu. Rev. Mater. Res. **37**, 387 (2007).
[5] Y. Tokura and S. Seki, Adv. Mater. **22**, 1554 (2010).
[6] T. Kimura *et al.*, Nature (London) **426**, 55 (2003).
[7] A. Malashevich and D. Vanderbilt, Phys. Rev. Lett. **101**, 037210 (2008).
[8] H. J. Xiang *et al.*, Phys. Rev. Lett. **101**, 037209 (2008).
[9] K. Taniguchi *et al.*, Phys. Rev. Lett. **97**, 097203 (2006).
[10] C. Tian *et al.*, Phys. Rev. B **80**, 104426 (2009).
[11] I. A. Sergienko and E. Dagotto, Phys. Rev. B **73**, 094434 (2006).

[12] H. Katsura, N. Nagaosa, and A. V. Balatsky, Phys. Rev. Lett. **95**, 057205 (2005).
[13] T. Kimura, J. C. Lashley, and A. P. Ramirez, Phys. Rev. B **73**, 220401(R) (2006).
[14] S. Seki *et al.*, Phys. Rev. B **75**, 100403(R) (2007).
[15] S. Seki, Y. Onose, and Y. Tokura, Phys. Rev. Lett. **101**, 067204 (2008).
[16] T. Kurumaji *et al.*, Phys. Rev. Lett. **106**, 167206 (2011).
[17] T. Arima, J. Phys. Soc. Jpn. **76**, 073702 (2007).
[18] C. Jia *et al.*, Phys. Rev. B **74**, 224444 (2006).
[19] T. Nakajima *et al.*, Phys. Rev. B **77**, 052401 (2008).
[20] See Supplemental Material at http://link.aps.org/supplemental/10.1103/PhysRevLett.107.157202 for the proofs of the stated relationships, the computational procedures for the parameter specifications, and the tight-binding analysis.